Fast Frequency Sweep Technique for Efficient Analysis of Dielectric Waveguides[1]

Sergey V. Polstyanko[2] Romanus Dyczij-Edlinger[3] Jin-Fa Lee[2]

Abstract

This paper describes a new approach to spectral response computation of an arbitrary 2D waveguide. This technique is based on the Tangential Vector Finite Element Method (TVFEM) in conjunction with the Asymptotic Waveform Evaluation (AWE) technique. The former is used to obtain modes characteristics for a central frequency, whereas the latter employs an efficient algorithm to compute frequency moments for each mode. These moments are then matched via Padé approximation to a reduced-order rational polynomial which can be used to interpolate mode over a frequency band with a high degree of accuracy. Furthermore, the moments computations and subsequent interpolation for a given set of frequency points can be done much more rapidly than just simple simulations for each frequency point.

1 Introduction

COMPUTER–AIDED numerical analysis has become a necessary tool for designing microwave and optical wave-guiding structures such as microstrip line, optical channel guide and optical fiber. Different numerical techniques have been presented in the past to solve a wide variety of dielectric waveguide problems [1, 2, 3, 4, 5]. Among them, the Finite Element Method (FEM) is probably the most versatile [6, 3, 7, 8]. By discretizing the waveguide cross-section into a number of triangles and employing the variational technique, the FEM can be used to predict the propagation characteristics of any arbitrary waveguide accurately.

It has been shown by previous researchers, that by using the Tangential Vector Finite Element Method (TVFEM) electromagnetic characteristics of propagating modes in waveguides can be obtained without the occurrences of so-called spurious solutions [9, 8, 10]. However, these spurious solutions are not completely eliminated, they are reduced to a set of identifiable non-physical solutions corresponding to the null-space of the generalized eigenmatrix equation. Consequently, they can slow down the convergence of desirable modes during the solution process and cause additional complications. In this paper, we have introduced an additional set of constraint equations for the generalized eigenmatrix equation. By using

[1]This work was sponsored by Hewlett-Packard Inc.

[2]The authors are with the ECE Department, WPI, Worcester, MA 01609 USA

[3]Currently with Motorola Inc., Schaumburg, IL

this set of constraint equations, the non-physical solutions can be completely suppressed and the solution space is limited only to physical modes.

Previously, we have implemented a $\mathcal{H}_0^1(curl)$ Tangential Vector Finite Element Method (TVFEM) to perform a full-wave analysis of an anisotropic waveguide which is characterized simultaneously by both off-diagonal second rank symmetric $[\epsilon]$ and $[\mu]$ tensors [11]. But if one wants to compute a dispersion curve with the propagation constant versus frequency over a given frequency band, this analysis has to be repeated for many sampling frequency points. Consequently, the entire process can become very time consuming, especially when the number of frequency points becomes large and the number of unknowns is significant.

To avoid this difficulty a new approach based on the Asymptotic Waveform Evaluation (AWE) [12] has been developed. Starting with the known modes characteristics for a central frequency, the AWE technique employs an efficient algorithm to compute frequency moments for each mode. These moments are then matched via Padé approximation to a reduced-order rational polynomial with a high degree of accuracy. Furthermore, the moments computations and subsequent interpolation for a given set of frequency points can be done more rapidly than just simple simulations for each frequency point. To verify the proposed approach, the method has been implemented and tested for sample wave-guiding structures and the resultant dispersion curves are compared with those obtained by the $\mathcal{H}_0^1(curl)$ TVFEM. The details of the formulation, error estimation, and sample numerical results will be discussed in the following sections.

2 Formulation

2.1 Time Harmonic Maxwell's Equations

Shown in Fig. 1 is a general wave-guiding structure that is uniform in the z direction with an arbitrary cross-section Ω in the xy plane and the boundary of Ω consists of either perfect electric conductor (PEC) or perfect magnetic conductor (PMC). Assuming time-harmonic excitations, Maxwell's equations can be written as

$$\begin{aligned} \nabla \times \vec{E} &= -j\omega\mu_0[\mu_r]\vec{H} \\ \nabla \times \vec{H} &= j\omega\epsilon_0[\epsilon_r]\vec{E} + [\sigma]\vec{E} \\ \nabla \cdot [\mu_r]\vec{H} &= 0 \\ \nabla \cdot [\epsilon_r]\vec{E} &= 0 \end{aligned} \tag{1}$$

where $[\epsilon_r]$ and $[\mu_r]$ are the relative permittivity and permeability,respectively, and $[\sigma]$ is the conductivity tensor. In the present study, they are assumed to be diagonal tensors. Furthermore, in the frequency domain, $[\epsilon_r]$ and $[\sigma]$ can be combined to define a complex effective relative permittivity $[\overline{\epsilon_r}]$ as

$$[\overline{\epsilon_r}] = [\epsilon_r] - \frac{j}{\omega\epsilon_0}[\sigma] \tag{2}$$

To solve for the wave propagation characteristics, we start by expressing the fields as

$$\begin{aligned} \vec{E}(\vec{r};t) &= \vec{\mathcal{E}}(x,y)e^{-\gamma z}e^{j\omega t} \\ \vec{H}(\vec{r};t) &= \vec{\mathcal{H}}(x,y)e^{-\gamma z}e^{j\omega t} \end{aligned} \tag{3}$$

where $\gamma = \alpha$ +j β is the propagation constant with α, β being the attenuation and phase constant, respectively; and $\vec{r} = (x, y, z)$ denotes the position vector of a point in the waveguide.

2.2 A-V Formulation

In the current formulation, we use a vector potential $\vec{A}$ and a scalar potential φ as our unknown variables. They are defined through the fields as

$$\begin{aligned} \vec{B} &= \nabla \times \vec{A} \\ \vec{E} &= -j\omega\vec{A} - c\nabla\varphi \end{aligned} \tag{4}$$

Also, it is well known that the vector potential $\vec{A}$ defined by (4) is not unique without imposing a gauge condition. Instead of using the conventional Coulomb or Lorenz gauge we choose $A_z = 0$. This condition will greatly simplify the formulation. By using Eqs. (1)-(4) and the gauge condition $A_z = 0$, Maxwell's equations become

$$\begin{aligned} \nabla \times [\nu]\nabla \times \vec{A}_\tau - k_0^2[\overline{\epsilon_r}]\vec{A}_\tau + jk_0[\overline{\epsilon_r}]\nabla\varphi = 0 \\ -jk_0\nabla \cdot [\overline{\epsilon_r}]\vec{A}_\tau - \nabla \cdot [\overline{\epsilon_r}]\nabla\varphi = 0 \end{aligned} \tag{5}$$

where $k_0 = \omega^2\epsilon_0\mu_0$ is the free-space wavenumber and $[\nu] = [\mu_r]^{-1}$ denotes the inverse matrix of $[\mu_r]$. Taking into account that $\nabla = \nabla_\tau$ - $\gamma\hat{z}$, equations (5) can be rewritten as

$$\nabla_\tau \times \mu_{zz}^{-1}\nabla_\tau \times \vec{A}_\tau - \gamma^2[\nu]_\tau\vec{A}_\tau - k_0^2[\overline{\epsilon_r}]_\tau\vec{A}_\tau + jk_0[\overline{\epsilon_r}]_\tau\nabla_\tau\varphi = 0 \tag{6}$$

$$-\gamma\nabla_\tau \cdot [\nu]_\tau\vec{A}_\tau - jk_0\gamma\overline{\epsilon}_{zz}\varphi = 0 \tag{7}$$

$$-jk_0\nabla_\tau \cdot [\overline{\epsilon_r}]_\tau\vec{A}_\tau - \nabla_\tau \cdot [\overline{\epsilon_r}]_\tau\nabla_\tau\varphi - \gamma^2\overline{\epsilon}_{zz}\varphi = 0 \tag{8}$$

where

$$[\overline{\epsilon_r}]_\tau = \begin{bmatrix} \overline{\epsilon}_{xx} & 0 \\ 0 & \overline{\epsilon}_{yy} \end{bmatrix} \quad [\nu]_\tau = \begin{bmatrix} \nu_{yy} & 0 \\ 0 & \nu_{xx} \end{bmatrix} \tag{9}$$

Equation (7) can be obtained by subtracting equation (8) from (6). Subsequently, in the current formulation, we focus on solving Eqs. (6) and (8) simultaneously. Furthermore, boundary conditions associated with this formulation are:
on PEC s

$$\begin{cases} \vec{n} \times \vec{A}_\tau = 0 \\ \varphi = 0 \end{cases} \tag{10}$$

on PMC s

$$\begin{cases} \vec{n} \times ([\nu]\nabla \times \vec{A}_\tau) = 0 \\ [\overline{\epsilon_r}]_\tau(jk_0\vec{A}_\tau + \nabla_\tau\varphi) \cdot \vec{n} = 0 \end{cases} \tag{11}$$

where $\vec{n}$ is the normal vector to the boundary.

3 Finite Element Implementation

3.1 The Bilinear Form

Equations (6), (8) and boundary conditions (10), (11) describe a well defined boundary value problem (BVP) and are ready for the application of the finite element method. Application of the Galerkin's method for the current BVP results in the following bilinear form

$$\begin{aligned} B(\vec{v},\vec{a}) &= \int_\Omega \{\mu_{zz}^{-1}(\nabla_\tau \times \vec{v}_\tau)\cdot(\nabla_\tau \times \vec{a}_\tau) - k_0^2 \vec{v}_\tau \cdot [\overline{\epsilon_r}]_\tau \vec{a}_\tau + \nabla_\tau v_z \cdot [\overline{\epsilon_r}]_\tau \nabla_\tau a_z \\ &+ jk_0 \vec{v}_\tau \cdot [\overline{\epsilon_r}]_\tau \nabla_\tau a_z + jk_0 \nabla_\tau v_z \cdot [\overline{\epsilon_r}]_\tau \vec{a}_\tau\} d\Omega \\ &- \gamma^2 \int_\Omega \{\vec{v}_\tau \cdot [\nu]_\tau \vec{a}_\tau + \overline{\epsilon}_{zz} v_z a_z\} d\Omega \end{aligned} \tag{12}$$

where $\vec{v}, \vec{a}$ are the testing and trial fields, respectively. Notice that in an effort to balance the smoothness requirements on both the trial and testing fields, we have adopted the Green's theorems to derive Eq. (12). Moreover, to facilitate our discussion, we have also employed a vector notation for the potentials as

$$\vec{a} = \begin{bmatrix} \vec{a}_\tau \\ a_z \end{bmatrix} = \begin{bmatrix} \vec{A}_\tau \\ \varphi \end{bmatrix} \tag{13}$$

Judging from the bilinear form (12), a vector field $\vec{a}$ is admissible in the bilinear form if and only if

$$\vec{a} \in V = \left\{ \vec{v} :\ \vec{v}_\tau \in (L_2(\Omega))^2;\ \nabla_\tau \times \vec{v}_\tau \cdot \hat{z} \in L_2(\Omega);\ v_z \in C^0(\Omega) \right\} \tag{14}$$

where $L_2(\Omega)$, $C^0(\Omega)$ are the sets of square integrable functions and continuous functions in Ω, respectively.

3.2 Two-dimensional $\mathcal{H}_0^1(curl)$ TVFEM

In the Galerkin's process, we need to find a complex number γ and a vector function $\vec{a} \in V$, such that $B(\vec{v},\vec{a}) = 0$ for every $\vec{v}$ in the infinite dimensional space V. The finite element method is nothing but replacing V by a sequence of finite dimensional subspaces V^h contained in V. In the present approach, we have chosen V^h to be spanned by the $\mathcal{H}_0^1(curl)$ TVFEM basis functions. Mathematically, we define a finite dimensional vector space $\mathcal{H}^k(curl;\Omega^h)$, for a two-dimensional discretization Ω^h as

$$\mathcal{H}^k(curl;\Omega^h) = (P_k(\Omega^h))^2 \oplus S_{k+1}(\Omega^h) \tag{15}$$

where $P_k(\Omega^h)$ is the set of piece-wise polynomials in Ω^h with order complete to k. The function space $S_{k+1}(\Omega^h)$ can be defined simply by

$$S_k(\Omega^h) = \left\{ \vec{v}_\tau^h \mid \vec{v}_\tau^h \in (\tilde{P}_k(\Omega^h))^2,\ < \vec{v}_\tau^h, \nabla_\tau \phi^h >= 0,\ \forall \phi \in \tilde{P}_{k+1}(\Omega^h) \right\} \tag{16}$$

and $\tilde{P}_k(\Omega^h)$ is the set of piece-wise homogeneous kth order polynomials in Ω^h. And the function space $\mathcal{H}_0^k(curl;\Omega^h)$ is further defined by

$$\mathcal{H}_0^k(curl;\Omega^h) = \left\{ \vec{v}_\tau^h \mid \vec{v}_\tau^h \in \mathcal{H}^k(curl;\Omega^h),\ \hat{n} \times \vec{v_\tau}^h = 0 \ on\ \Gamma_{PEC} \right\} \tag{17}$$

Henceforth, the finite dimensional space V^h that is used in the current FEM formulation is

$$V^h = \left\{ \vec{v}^{\,h} \mid \vec{v_\tau}^{\,h} \in \mathcal{H}_0^1(curl;\Omega^h),\ v_z^h \in P_2(\Omega^h),\ v_z^h = 0\ on\ \Gamma_{PEC} \right\} \tag{18}$$

Note that in choosing the FEM space as in (18), the following statement is valid: $\forall \vec{v}^{\,h} \in V^h$ we have $\nabla v_z^h \in \mathcal{H}_0^1(curl;\Omega^h)$. Explicitly, for a tetrahedral element there are 8 vector basis functions and 6 scalar basis functions for the finite element space V^h (Fig. 2). Each trial/testing function $\vec{a}^{\,h} \in V^h$ can now be written as

$$\vec{a_\tau}^{\,h} = \sum_{i=0}^{7} a_{\tau i}^h \vec{W}_i^h \qquad\qquad a_z^h = \sum_{i=0}^{5} a_{zi}^h \psi_i^h \tag{19}$$

where the 6 scalar basis functions ψ_i are the usual second order FEM basis functions, namely

$$\begin{aligned} \psi_0 &= 2\xi_0(\xi_0 - 1/2); & \psi_3 &= 4\xi_1\xi_2; \\ \psi_1 &= 2\xi_1(\xi_1 - 1/2); & \psi_4 &= 4\xi_0\xi_2; \\ \psi_2 &= 2\xi_2(\xi_2 - 1/2); & \psi_5 &= 4\xi_0\xi_1; \end{aligned}$$

and the 8 vector basis functions are given by

$$\begin{aligned} \vec{W}_0 &= \xi_1\nabla\xi_2 - \xi_2\nabla\xi_1; & & \\ \vec{W}_1 &= \xi_1\nabla\xi_2 + \xi_2\nabla\xi_1; & & \\ \vec{W}_2 &= \xi_2\nabla\xi_0 - \xi_0\nabla\xi_2; & \vec{W}_6 &= 4\xi_1(\xi_2\nabla\xi_0 - \xi_0\nabla\xi_2); \\ \vec{W}_3 &= \xi_2\nabla\xi_0 + \xi_0\nabla\xi_2; & \vec{W}_7 &= 4\xi_2(\xi_0\nabla\xi_1 - \xi_1\nabla\xi_0); \\ \vec{W}_4 &= \xi_0\nabla\xi_1 - \xi_1\nabla\xi_0; & & \\ \vec{W}_5 &= \xi_0\nabla\xi_1 + \xi_1\nabla\xi_0; & & \end{aligned}$$

where ξ_i is the Lagrangian interpolation polynomial or simplex coordinate at vertex i [13].

3.3 Generalized Eigenmatrix Equation

Finally, a generalized eigenmatrix equation can be obtained by setting $B(\vec{v},\vec{a}) = 0$ for every $\vec{v}^{\,h} \in V^h$. The result is

$$\sum_{\Omega_e} \left(\begin{bmatrix} [A]_e & [C]_e \\ [C]_e^T & [D]_e \end{bmatrix} \right) \begin{bmatrix} \underline{a}_\tau \\ \underline{a}_z \end{bmatrix} = \gamma^2 \sum_{\Omega_e} \left(\begin{bmatrix} [B]_e & 0 \\ 0 & [E]_e \end{bmatrix} \right) \begin{bmatrix} \underline{a}_\tau \\ \underline{a}_z \end{bmatrix} \tag{20}$$

where $\sum_{\Omega_e}$ means the summation over the contributions from each element and $\underline{a}_\tau, \underline{a}_z$ are the corresponding coefficient vector for the finite dimensional approximation of $\vec{a}^{\,h}$. Moreover, the element matrices in Eq. (20) are given by

$$\begin{aligned} [A]_e &= \int_{\Omega_e} \{\mu_{zz}^{-1}(\nabla_\tau \times \vec{W}_i)\cdot(\nabla_\tau \times \vec{W}_j) - k_0^2 \vec{W}_i \cdot [\overline{\epsilon_r}]_\tau \vec{W}_j\} d\Omega \\ [B]_e &= \int_{\Omega_e} \{\vec{W}_i \cdot [\nu]_\tau \vec{W}_j\} d\Omega \\ [C]_e &= jk_0 \int_{\Omega_e} \{\vec{W}_i \cdot [\overline{\epsilon_r}]_\tau \nabla_\tau \psi_j\} d\Omega \\ [D]_e &= \int_{\Omega_e} \{\nabla_\tau \psi_i \cdot [\overline{\epsilon_r}]_\tau \nabla_\tau \psi_j\} d\Omega \\ [E]_e &= \int_{\Omega_e} \{\epsilon_{zz}\psi_i\psi_j\} d\Omega \end{aligned} \tag{21}$$

The integrations in (21) are performed on triangular regions. To make computation faster we rearrange the matrix equation (20) into

$$\begin{bmatrix} [B] & 0 \\ 0 & [E] \end{bmatrix} \begin{bmatrix} \underline{a}_\tau \\ \underline{a}_z \end{bmatrix} = \frac{1}{\gamma^2+\theta^2} \left(\begin{bmatrix} [A] & [C] \\ [C]^t & [D] \end{bmatrix} + \theta^2 \begin{bmatrix} [B] & 0 \\ 0 & [E] \end{bmatrix} \right) \begin{bmatrix} \underline{a}_\tau \\ \underline{a}_z \end{bmatrix} \tag{22}$$

where $[A] = \sum_{\Omega_e} [A]_e$ and so on, and $\theta^2 = k_0^2 \cdot \mu_{max} \cdot \epsilon_{max}$ is an educated guess, which can be obtained by a quasi-TEM approximation for an isotropic medium. The reason for this transformation is as follows: in a lossless dielectric waveguide, a more dominant mode corresponds to smaller γ^2 value and as a result, the $1/(\gamma^2+\theta^2)$ ratio will be larger. It turns out, that although the Lanczos algorithm can compute both the smallest and the largest eigenvalues, the latter almost always converges faster than the former one. Furthermore, from (21)and (22), we can conclude that for an anisotropic waveguide, characterized by diagonal permittivity and permeability tensors, the generalized eigenmatrix equation involves two complex but symmetric matrices. Subsequently, savings in computational time and storage can be realized by taking advantage of this symmetry.

3.4 Constraint Equations

The eigenpair solutions $< \gamma_i, \vec{a}^{\,i} >$ to Eq. (22) can be divided into three groups. This can be seen as follows: Our bilinear form (12) and subsequently the generalized eigenmatrix equation (22) are derived based on Eqs. (6) and (8). The solutions of (6) and (8) are guaranteed to be nontrivial solutions of Maxwell's equations only if $\gamma \neq 0$. When $\gamma = 0$, there are two possibilities: the cutoff modes which are still solutions of Maxwell's equations; and the trivial solutions : $\vec{a} = \begin{bmatrix} \vec{A}_\tau \\ \varphi \end{bmatrix} \neq 0$, but $\vec{E} = -j\omega\vec{A}_\tau - c\nabla\varphi = 0$. To summarize, the eigenpairs $< \gamma_i, \vec{a}^{\,i} >$ can be divided into 3 groups

group 1 (physical modes): $\gamma_i \neq 0$, $\vec{E}_i = -j\omega\vec{A}_\tau^{\,i} - c\nabla\varphi^i \neq 0$;
group 2 (cutoff modes): $\gamma_i = 0$, $\vec{E}_i = -j\omega\vec{A}_\tau^{\,i} - c\nabla\varphi^i \neq 0$;
group 3 (trivial modes): $\gamma_i = 0$, $\vec{E}_i = -j\omega\vec{A}_\tau^{\,i} - c\nabla\varphi^i = 0$.

Our objective is to develop a constrained Lanczos algorithm which will solve for solutions in group 1 and 2 without the occurrences of group 3. To achieve this goal, we first notice that the group 3 solutions form a vector function space V_{NULL}^h defined as

$$V_{NULL}^h = \left\{ \begin{bmatrix} \vec{v}_\tau \\ v_z \end{bmatrix} : \ \vec{v}_\tau = \tfrac{j}{k_0}\nabla_\tau v_z \right\} \tag{23}$$

and obviously $V_{NULL}^h \subset V^h$. Furthermore, the number of trivial modes, or the dimension of V_{NULL}^h equals the number of free nodes in the second order discretization. Although these trivial solutions can be easily identified and disregarded at the post-processing stage, their presence can significantly degrade the performance of the Lanczos algorithm. Therefore, a constrained Lanczos algorithm which completely suppresses the occurrence of these trivial modes will enhance the numerical efficiency and stability.

3.5 Orthogonality Relations

From Eq. (12), the following orthonormal property exists for the eigensolutions:

$$\int_\Omega (\vec{a}_\tau^{\,i} \cdot [\nu]_\tau \vec{a}_\tau^{\,j} + \overline{\epsilon}_{zz} a_z^i a_z^j) = \delta_{ij} \tag{24}$$

where δ_{ij} is the Kronecker delta-function. Equation (24) is the basis for the constraint equation that will be used in the constrained Lanczos algorithm. Since a physical solution $\vec{a}^{\,j}$ from group 1 or group 2 must be orthogonal to any $\vec{a}^{\,i} \in V_{NULL}^h$ through Eq. (24), the constraint equation for the physical solutions reads

$$\int_\Omega \{\frac{j}{k_0} \nabla_\tau \upsilon_z \cdot [\nu]_\tau \vec{a}_\tau + \epsilon_{zz} \upsilon_z a_z\} d\Omega = 0 \quad \forall \upsilon_z \in P_2(\Omega),\ \upsilon_z = 0\ on\ \Gamma_{PEC} \tag{25}$$

In discretized form equation (25) reduces to the following matrix equation

$$a_z = -[E]^{-1}[F] a_\tau \tag{26}$$

where matrices $[E]$ and $[F]$ are given by

$$\begin{aligned} [E]_e &= \int_{\Omega_e} \{\epsilon_{zz} \psi_i \psi_j\} d\Omega \\ [F]_e &= \frac{j}{k_0} \int_{\Omega_e} \{\nabla_\tau \psi_i \cdot [\nu]_\tau \vec{W}_j\} d\Omega \end{aligned} \tag{27}$$

Equation (26) can be used as a set of additional constraints to restrict the solution space to group 1 and 2 solutions in the Lanczos algorithm.

3.6 Constrained Lanczos Algorithm

By incorporating the constraint equation (26) into the generalized algorithm, the following algorithm can be used to find N eigenpairs of the generalized eigenmatrix equation $[A]x = \lambda[B]x$ without the occurrences of group 3 solutions

1. Input the number of desired modes N.
2. Input an initial guess x^0, and
   (a) $\bar{x}_\tau^{\,0} = x_\tau^0$, $\bar{x}_z^{\,0} = -[E]^{-1}[F]\bar{x}_\tau^{\,0}$;
   (b) $g_0 = [B]\bar{x}^{\,0}$.
3. Orthogonalize g_0 to previously converged vectors $X_i (i = 1, ...n)$,

$$\bar{g}_0 = g_0 - \sum_i^n c_i X_i, \quad c_i = X_i^T g_0 \tag{28}$$

4. Solve $[B]x^1 = \bar{g}_0$ and normalize x^1 to obtain $v_1 = \frac{x^1}{\|x^1\|}$ (m = 1).

5. $f = [A]v_m - h_{m,m}[B]v_m - h_{m-1,m}[B]v_{m-1}$, where

$$h_{m,m} = \frac{v_m^T[A]v_m}{v_m^T[B]v_m}; \quad h_{m-1,m} = \frac{v_{m-1}^T[A]v_m}{v_{m-1}^T[B]v_{m-1}}.$$

6. Orthogonalize f to previously converged vectors $X_i (i = 1, ...n)$, namely

$$\bar{f} = f - \sum_{i=1}^{n} d_i X_i, \quad d_i = X_i^T f \tag{29}$$

7. Solve for x^{m+1} from $[B]x^{m+1} = \bar{f}$, and

   (a) $\bar{x}_\tau^{m+1} = x_\tau^{m+1}$, $\bar{x}_z^{m+1} = -[E]^{-1}[F]\bar{x}_\tau^{m+1}$;

   (b) $h_{m+1,m} = \|\bar{x}^{\,m+1}\|$, $v_{m+1} = \frac{\bar{x}^{\,m+1}}{\|\bar{x}^{\,m+1}\|}$.

8. Calculate $(\lambda^{(m)}, y^{(m)})$ of the triangular matrix $\mathcal{H}_m$ where

$$\mathcal{H}_m = \begin{bmatrix} h_{1,1} & h_{1,2} & & & & \\ h_{2,1} & h_{2,2} & h_{2,3} & & & \\ & h_{3,2} & h_{3,3} & & & \\ & & & \ldots & & \\ & & & & h_{m,m-1} & h_{m,m} \end{bmatrix} \tag{30}$$

9. Check the residual norm $= h_{m+1,m} \left| y_m^{(m)} \right|$ for convergence; if not converged, increment m by 1 and go to step 4.

10. Increment n by 1. If all desired modes have converged ($n = N$) then stop, otherwise go to step 1.

We would like to comment here that theoretically if the initial vector is constructed in such a way that it satisfies equation (26) our solution becomes orthogonal to the subspace of trivial solutions. The purpose of step 7(a) is simply to avoid the accumulation of rounding error. Practically, step 7(a) can be performed selectively.

4 Asymptotic Waveform Evaluation

It has been shown previously that the FEM formulation for the electromagnetic wave propagation in 2D wave-guiding structures leads to the matrix equation of the form

$$\mathcal{P}(f)x(f) = \lambda(f)\mathcal{Q}(f)x(f) \tag{31}$$

where $\mathcal{P}(f)$ and $\mathcal{Q}(f)$ are the square complex matrices, f is a given frequency, x represents the unknown field components, and λ is related to the propagation constant itself. Equation (31) can be solved directly for the unknown eigenpairs $< \lambda_i, x_i >$ by using the constrained

Lanczos algorithm described above. However, if we are looking for the solution over a given frequency band $[f^0, f^1]$ the entire process has to be repeated for a set of frequencies $\{f_i\}_{i=0}^{i=N}$ such that $f^0 = f_0 < f_1 < \cdots < f_N = f^1$ to find eigenpairs $< \lambda_i, x_i >$. After that the eigenpair $< \lambda(f), x(f) >$ for any arbitrary frequency f within the interval $[f^0, f^1]$ can be determined based on an interpolation technique such as linear, quadratic or spline approximation.

However, if we deal with a big problem or the number of sampling points N is large, then the entire analysis can become very time consuming. Consequently, our goal is to develop an alternative method for which the spectral responses over a given frequency range can be determined efficiently.

To achieve the above goal, a Fast Frequency Sweep (FFS) technique is proposed and implemented in this work. The FFS approach proposed herein is a combination of the TVFEM, described in previous sections, and the Asymptotic Waveform Evaluation (AWE) technique. The latter has been successfully used for the analysis/simulation of 2D/3D interconnect structures on integrated circuits and has recently gained much attention from the CAD community [12, 14, 15, 16]. A number of papers have devoted to AWE as the method for computing an approximation of the response of a linear circuit from circuit's low-order moments. Furthermore, the method has been proven by many researchers to be an efficient and accurate technique for simulating lumped, linear circuit of arbitrary topologies.

Recently, several attempts have also been made to apply the AWE technique for electomagnetic problems and the validity of the approach has been shown [17, 18]. In this paper we extend the AWE method, based on the rational function approximation, for modeling wave propagation in 2D wave-guiding structures. Furthermore, we will compare the power series expansion and rational function approximation and present the results of our accuracy study.

4.1 Taylor Expansion

We start our discussion with the following generalized eigenmatrix equation that was obtained previously

$$\begin{bmatrix} [A] & [C] \\ [C]^T & [D] \end{bmatrix} \begin{bmatrix} \vec{A}_\tau \\ \varphi_z \end{bmatrix} = \gamma^2 \begin{bmatrix} [B] & 0 \\ 0 & [E] \end{bmatrix} \begin{bmatrix} \vec{A}_\tau \\ \varphi_z \end{bmatrix} \tag{32}$$

where the element matrices are the same as those given by Eq. (21). To facilitate our discussion, we simply rewrite (32) as

$$\mathcal{P}(k)x(k) = \lambda(k)\mathcal{Q}(k)x(k) \tag{33}$$

where matrices $\mathcal{P}(k)$, $\mathcal{Q}(k)$ and eigenpairs $< \lambda(k), x(k) >$ are in general functions of the wavenumber k,

$$\mathcal{P}(k) = \begin{bmatrix} [A] & [C] \\ [C]^T & [D] \end{bmatrix}; \quad \mathcal{Q}(k) = \begin{bmatrix} [B] & 0 \\ 0 & [E] \end{bmatrix}; \quad x(k) = \begin{bmatrix} \vec{A}_\tau \\ \varphi_z \end{bmatrix} \tag{34}$$

Let us first expand these quantities by Taylor series around $k = k_0$. Namely,

$$\begin{aligned} \mathcal{P}(k) &= \sum_{i=0}^{N} \mathcal{P}_i (k-k_0)^i \qquad & \mathcal{Q}(k) &= \sum_{i=0}^{N} \mathcal{Q}_i (k-k_0)^i \\ \lambda(k) &= \sum_{i=0}^{N} \lambda_i (k-k_0)^i \qquad & x(k) &= \sum_{i=0}^{N} x_i (k-k_0)^i \end{aligned} \tag{35}$$

Furthermore, from Eq. (21) it can be seen that matrix $\mathcal{Q}(k)$ has only the $\mathcal{Q}_0$ component, whereas matrix $calP(k)$ has contributions from $\mathcal{P}_0, \mathcal{P}_1, \mathcal{P}_2$. Substituting equations (35) into (33) and matching the coefficients of corresponding power of $(k - k_0)$ we end up with the following recursive system of equations to solve

$$\begin{aligned} 1: &\quad (\mathcal{P}_0 - \lambda_0 \mathcal{Q}_0) x_1 = \mathcal{Q}_0 \lambda_1 x_0 - \mathcal{P}_1 x_0 \\ &\quad \cdots\cdots\cdots\cdots\cdots\cdots\cdots\cdots \\ i: &\quad (\mathcal{P}_0 - \lambda_0 \mathcal{Q}_0) x_i = \mathcal{Q}_0 (\lambda_i x_0 + \cdots + \lambda_1 x_{i-1}) - \mathcal{P}_2 x_{i-2} - \mathcal{P}_1 x_{i-1} \\ &\quad \cdots\cdots\cdots\cdots\cdots\cdots\cdots\cdots \\ N: &\quad (\mathcal{P}_0 - \lambda_0 \mathcal{Q}_0) x_N = \mathcal{Q}_0 (\lambda_N x_0 + \cdots + \lambda_1 x_{N-1}) - \mathcal{P}_2 x_{N-2} - \mathcal{P}_1 x_{N-1} \end{aligned} \tag{36}$$

Taking into account that x_0 is the eigenvector of (33) and multiplying (36) by x_0^T, λ_i and consequently x_i can be found. In this process, we have to solve the symmetric eigenmatrix equation (32) only once for the central frequency point. After that the corresponding Taylor series expansion is found by solving (36) with the same matrix $(\mathcal{P}_0 - \lambda_0 \mathcal{Q}_0)$ but different right-hand sides. This process can be performed efficiently once the factorization of matrix $(\mathcal{P}_0 - \lambda_0 \mathcal{Q}_0)$ becomes available.

4.2 Padé Expansion

In many cases, the Taylor series expansion for the solution of eigenmatrix equation (32) gives fairly good results. However the situation is different if one wants to find an approximate solution in the proximity of a pole or some other singularity of the desirable function. In such cases, Taylor expansion fails to converge, whereas rational interpolation may still provide satisfactory results. Subsequently, we may want to replace the Taylor expansion by the so-called Padé expansion to improve the accuracy of our numerical solution. In this section we explain how to construct a rational function for the eigenvalue $\lambda(k)$. The extension of this approach to the eigenvector is straight-forward and is not given here. Using the Taylor expansion we can express an eigenvalue $\lambda(k)$ as

$$\lambda(k) = \sum_{i=0}^{N} \lambda_i (k-k_0)^i \tag{37}$$

whereas in the Padé expansion we employ a rational polynomial Λ to interpolate $\lambda(k)$ as,

$$\Lambda(k) = \frac{\sum_{i=0}^{L} p_i (k-k_0)^i}{1 + \sum_{i=1}^{M} q_i (k-k_0)^i} \tag{38}$$

The rational function Λ is defined by its $L+M+1$ coefficients to be determined later. For a given amount of computational effort, one can usually construct a rational approximation that has a smaller error than a polynomial approximation. Furthermore, for a fixed value of $L+M$ the error is the smallest when $P_L(k)$ and $Q_M(k)$ have the same degree or $P_L(k)$ has a degree one higher than $Q_M(k)$. We construct the rational polynomial $\Lambda(k)$ in such a way that it agrees with $\lambda(k)$ at k_0 and their derivative up to $L+M$ degree at $k=k_0$. These conditions result in a system of $L+M+1$ linear equations to solve. Namely,

$$\begin{aligned} \lambda_0 - p_0 &= 0 \\ q_1\lambda_0 + \lambda_1 - p_1 &= 0 \\ q_2\lambda_0 + q_1\lambda_1 + \lambda_2 - p_2 &= 0 \\ \cdots\cdots\cdots\cdots\cdots\cdots\cdots\cdots & \\ q_M\lambda_{L-M} + q_{M-1}\lambda_{L-M+1} + \cdots + \lambda_L - p_L &= 0 \end{aligned} \tag{39}$$

and

$$\begin{aligned} q_M\lambda_{L-M+1} + q_{M-1}\lambda_{L-M+2} + \cdots + q_1\lambda_L + \lambda_{L+1} &= 0 \\ q_M\lambda_{L-M+2} + q_{M-1}\lambda_{L-M+3} + \cdots + q_1\lambda_{L+1} + \lambda_{L+2} &= 0 \\ \cdots\cdots\cdots\cdots\cdots\cdots\cdots\cdots & \\ q_M\lambda_L + q_{M-1}\lambda_{L+1} + \cdots + q_1\lambda_{L+M-1} + \lambda_{L+M} &= 0 \end{aligned} \tag{40}$$

The M equations in (40) involve only the unknowns $q_1,\ldots,q_M$ and thus must be solved first. Then equations in (39) are used to find $p_0,\ldots,p_L$. Once $q_1,\ldots,q_M$ and $p_0,\ldots,p_L$ are determined Eq. (38) can be used to compute the propagation constant γ at any frequency. The described above procedure can be repeated to interpolate each component of the eigenvector $x(k)$.

5 Numerical Results

To validate the proposed approach several examples have been studied. In our first example we applied the Fast Frequency Sweep (FFS) method to a partially filled isotropic waveguide. Then, the method was tested on an anisotropic waveguide. Finally, a shielded microstrip line and a coplanar waveguide were considered. For each example a dispersion curve with the propagation constant versus frequency has been computed. The results were compared with the solution obtained by using the TVFEM for different frequency points. Furthermore, to perform an accuracy study of the proposed method over a frequency range we define the error by

$$error = \frac{|\mathcal{P}(k)x(k) - \lambda(k)\mathcal{Q}(k)x(k)|}{|x(k)|} \tag{41}$$

where $\mathcal{P}(k)$, $\mathcal{Q}(k)$ are the exact matrices from equation (33) and $\lambda(k)$, $x(k)$ are our approximate solutions. To compare the performance of Taylor and Padé expansions, we have plotted the error versus frequency for each example and comparisons have also been made.

5.1 Partially Filled Waveguide

To verify the proposed FFS method we have studied first a rectangular waveguide partially loaded with a dielectric, which is a well-known example that has been analyzed by many researchers. For the geometry shown in the inset of Fig. 3 the cutoff frequency of the dominant mode equals $31MHz$. Our objective was to demonstrate that the FFS method can predict correctly mode characteristics below the cutoff frequency.

First, we have used the $\mathcal{H}_0^1(curl)$ method to plot the reference dispersion curve for the dominant mode over the frequency interval from $1MHz$ to $140MHz$ (Fig. 3). After that, the FFS technique have been applied for the dominant mode starting with the known mode characteristics for $f_0 = 70MHz$. Two dispersion curves, computed by Taylor and Padé expansions, have been obtained and plotted in Fig. 3 for $f \in [1MHz, 140MHz]$. From Fig. 3 one can conclude that for frequencies smaller than $31MHz$ the dominant solution becomes an attenuating mode, but still Padé approximation has a good agreement with the reference curve. On the other hand, power series expansion fails for frequencies smaller than the cutoff. Error analysis, based on Eq. (41), only confirms the above conclusion and suggests that in general Padé expansion may have a potential advantage over Taylor expansion for physical problems with complex zeros and poles.

5.2 Anisotropic Waveguide

In this example we study a rectangular waveguide, which is loaded with an anisotropic rectangular insert (Fig. 5). The dielectric is made of TiO_2, a material having a very high permittivity $\epsilon_{rx} = 170$ and $\epsilon_{ry} = \epsilon_{rz} = 85$. The interest in this problem arose in connection with the realization of maser amplifiers in the high frequency region.

Our objective for this example was to demonstrate that the FFS technique proposed herein is able to predict multi-modes characteristics based on one central frequency point. Reference solutions for this structure have been obtained by using the $\mathcal{H}_0^1(curl)$ TVFEM (Fig. 5). The FFS approach has been applied to the waveguide for the central frequency $f_0 = 36MHz$, and solutions have been plotted in Fig. 5 and compared with reference results. Furthermore, the error analysis for the first two dominant modes is presented in Figs. 6-7 and again Padé expansion results in a better approximation over the entire frequency range.

5.3 Shielded Microstrip Line

The next example in this paper is a shielded microstrip transmission line. Figure 8 shows a sample microstrip line with strip which is assumed to be an infinitely-thin perfect electric conductor. The dominant mode, which is used for transmission purposes, is the one having a zero cutoff frequency. At cutoff, it reduces to a transverse electric and magnetic mode.

The solution procedure starts by solving for the normalized propagation constant by using the $\mathcal{H}_0^1(curl)$ TVFEM. After that the FFS analysis was carried out for the central

frequency $f_0 = 200MHz$. Both Taylor and Padé expansions have been obtained from $1MHz$ to $500MHz$, and results are plotted in Fig. 8. Shown results as well as the error analysis in Fig. 9 prove that the rational polynomial approximation is more accurate than the power series expansion. For example, even though both approachers fail near DC, Padé expansion agrees very well for high frequencies, whereas Taylor expansion does not. Moreover, at the lower frequency end, although Padé expansion fails eventually, its validity extends much further than for the power series expansions.

5.4 Coplanar Waveguide

Coplanar waveguide (CPW) structures have been attracting considerable attention because of their suitability for broad-band microwave integrated circuits (MIC's) and microwave monolithic integrated circuits (MMIC'c) as well as the ease of incorporation of series and shunt elements. In the last example in this paper, we study the dispersion characteristics of a conductor-backed coplanar waveguide (CBCPW) in a metal enclosure. The dispersion characteristics are computed for three modes using the proposed FFS procedure.

The structure is enclosed in a perfectly conducting channel and assumed to be uniform and infinite in the z direction. Both the ground plane and central strips are assumed to be perfectly conducting and infinitely thin, and the dielectric substrate is assumed to be lossless. For this example the comparison between the reference solutions and FFS solutions, for the central frequency $f_0 = 35MHz$, is presented in Fig. 10. In Fig. 10 we include only results of Padé expansion since they are much more accurate than those of Taylor expansion.

From all examples in this section we can conclude that, in general, the FFS procedure provides a good approximation for mode characteristics and may be used in the future for efficient computations of waveguide modes.

6 Concluding Remarks

In this paper we have described a novel approach to efficiently compute the spectral responses of arbitrary waveguides. The proposed technique is based on the Tangential Vector Finite Element Method in conjunction with the Asymptotic Waveform Evaluation approach. In the FEM computation, we have also developed a modified Lanczos algorithm with an additional set of constraint equations to completely eliminate non-physical solutions during the iteration process. This algorithm was combined with the $\mathcal{H}_0^1(curl)$ TVFEM to obtain electromagnetic characteristics of propagating modes in waveguides for any given frequency point. To result in a frequency response for a given frequency range, the frequency moments for each mode are computed through a recursive procedure. Note that, in this recursive procedure, the matrix does not change only the right-hand side has to be updated. Thus, the moments calculations become inexpensive when the factorization of the matrix is available. These moments are then matched via Padé approximation to a reduced-order rational polynomial which can be used to interpolate mode over a frequency band with a high degree of accuracy. Numerical results have shown that the $\mathcal{H}_0^1(curl)$ TVFEM when used together with AWE provides an efficient procedure for modeling two-dimensional wave-guiding structures.

References

[1] K. S. Kunz, and K. M. Lee. "A Three Dimensional Finite Difference Solution of the External Response of an Aircraft to a Complex Transient EM Enviroment: Part I – The method and its Implementation". *IEEE Trans. Electromagn. Compat.*, **20**:pp. 328–333, 1978.

[2] E. Schwig and W. B. Bridges. "Computer Analysis of Dielectric Waveguides: A Finite Difference Method". *IEEE Trans. Microwave Theory Tech.*, **32**(5):pp. 531–541, 1984.

[3] B. M. A. Rahman, and J. B. Davies. "Finite-Element Analysis of Optical and Microwave Problems". *IEEE Trans. Microwave Theory Tech.*, **32**:pp. 20–28, 1984.

[4] K. S. Yee. "Numerical Solution of Initial Boundary Value Problems Involving Maxwell's Equations in Isotropic Media". *IEEE Trans. Antennas Prop.*, **14**:pp. 302–307, 1966.

[5] M. D. Feit and J. A. Fleck. "Light Propagation in Graded-Index Optical Fibers". *Appl. Opt.*, **17**:pp. 3990–3998, 1978.

[6] B. Dillon, A. Gibson, J. Webb. "Cut-off and Phase Constant of Partially Filled Axially Magnetized, Gyromagnetic Waveguide Using Finite Elements". *IEEE Trans. Microwave Theory Tech.*, **41**(5):pp. 803–807, 1993.

[7] P. Vandenbulcke and P. E. Lagasse. "Eigenmode Analysis of Anisotropic Optical Fibers or Integrated Optical Waveguides". *Electronics letters*, **12**(5):pp. 120–121, 1976.

[8] J. Lee, D. Sun, Z. Cendes. "Full-Wave Analysis of Dielectric Waveguides Using Tangential Vector Finite Elements". *IEEE Trans. Microwave Theory Tech.*, **39**(8):pp. 1262–1271, 1991.

[9] Jin-Fa Lee. "Finite Element Analysis of Lossy Dielectric Waveguide". *IEEE Trans. Microwave Theory Tech.*, **42**(6):pp. 1025–1031, 1994.

[10] S. H. Wong and Z. J. Cendes. "Combined Finite Element-Modal Solution of Three-Dimensional Eddy Current Problems". *IEEE Trans. on Mag.*, **24**(6):pp. 2685–2687, 1988.

[11] S. V. Polstyanko and J.-F. Lee. "$H_1(curl)$ Tangential Vector Finite Element Method for Modeling Anisotropic Optical Fibers". *J. Lightwave Technol.*, **13**(11):pp. 2290–2295, 1995.

[12] J. E. Bracken, V. Raghvan and R. A. Rohrer. "Interconnect Simulation with Asymptotic Waveform Evaluation (AWE)". *IEEE Trans. on Circuits and Systems*, **39**(11):pp. 869–878, 1992.

[13] J. Jin. *The Finite Element Method in Electromagnetics*. John Wiley & Sons, Inc, 1993.

[14] R. Kao, and M. Horowitz. "Eliminating Redundant DC Equations for Asymptotic Waveform Evaluation". *IEEE Trans. Computer-Aided Design*, **13**(3):pp. 396–397, 1994.

[15] S. Kumashiro, R .A. Rohrer, and A. J. Strojwas. "Asymptotic Waveform Evaluation for Transient Analysis of 3-d Interconnect Structures". *IEEE Trans. Computer-Aided Design*, **12**(7):pp. 988–996, 1993.

[16] L. T. Pillage, and R. A. Rohrer. "Asymptotic Waveform Evaluation for Timing Analysis". *IEEE Trans. Computer-Aided Design*, **9**(4):pp. 352–366, 1990.

[17] M. Kuzuoglu, R. Mittra, J. Brauer, and G. Lizalek. "An Efficient Scheme for Finite Element Analysis in the Frequency Domain". volume **2**, pages pp. 1210–1219, 1996.

[18] E. K. Miller. "Model–Based Parameter Estimation in Electromagnetics: II–Applications to EM Observables". *ACES Newsletter*, **11**(1):pp. 35–56, 1996.

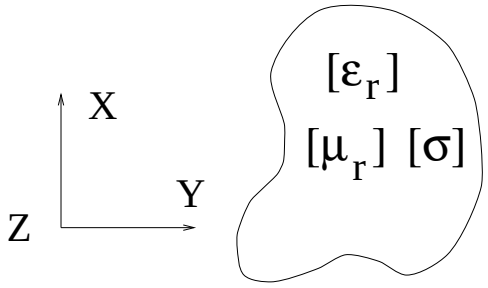

Figure 1: General anisotropic optical waveguide

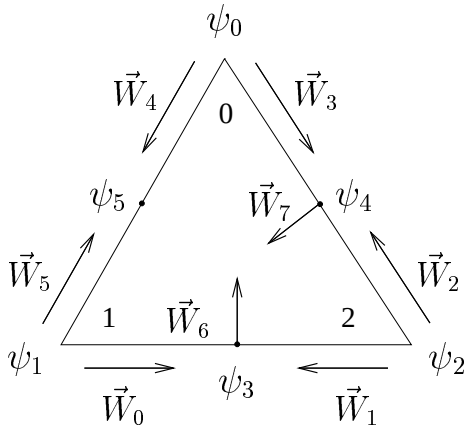

Figure 2: Two dimensional $\mathcal{H}_0^1(curl)$ tangential vector element.

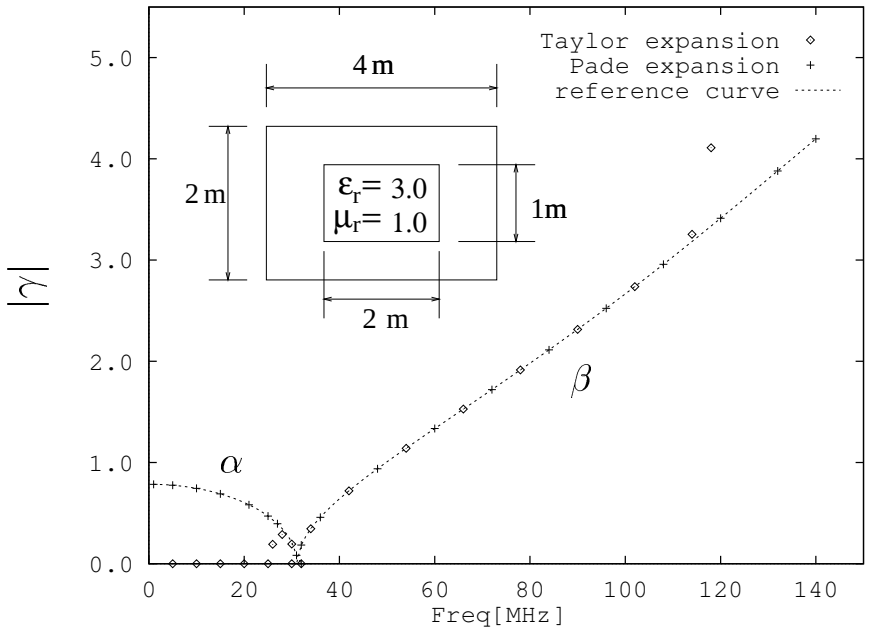

Figure 3: Dispersion curve of the fundamental mode for the partially filled waveguide. Central frequency has been chosen to be $f_0 = 70$[MHz]. Inset shows a dielectric waveguide filled with an isotropic material.

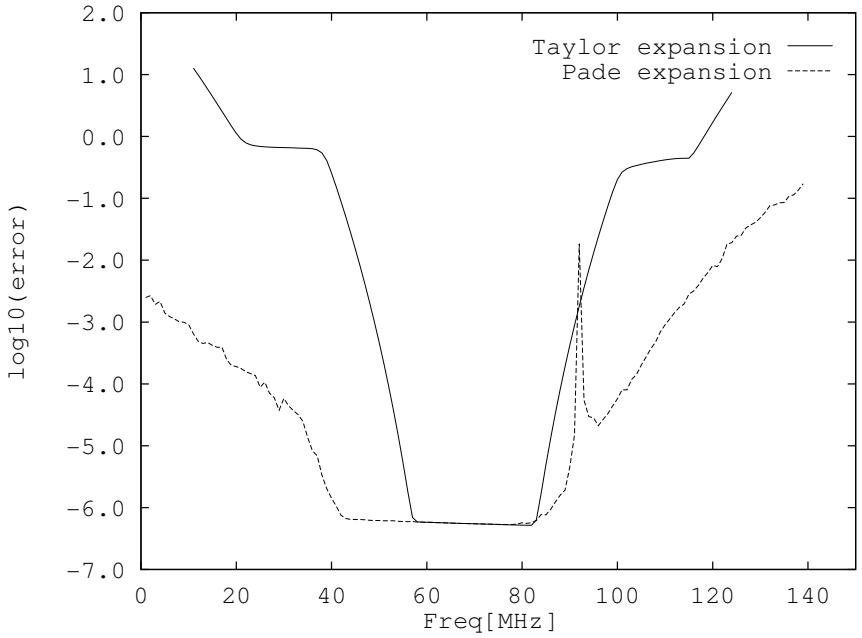

Figure 4: Error versus frequency for the central frequency $f_0 = 70$[MHz].

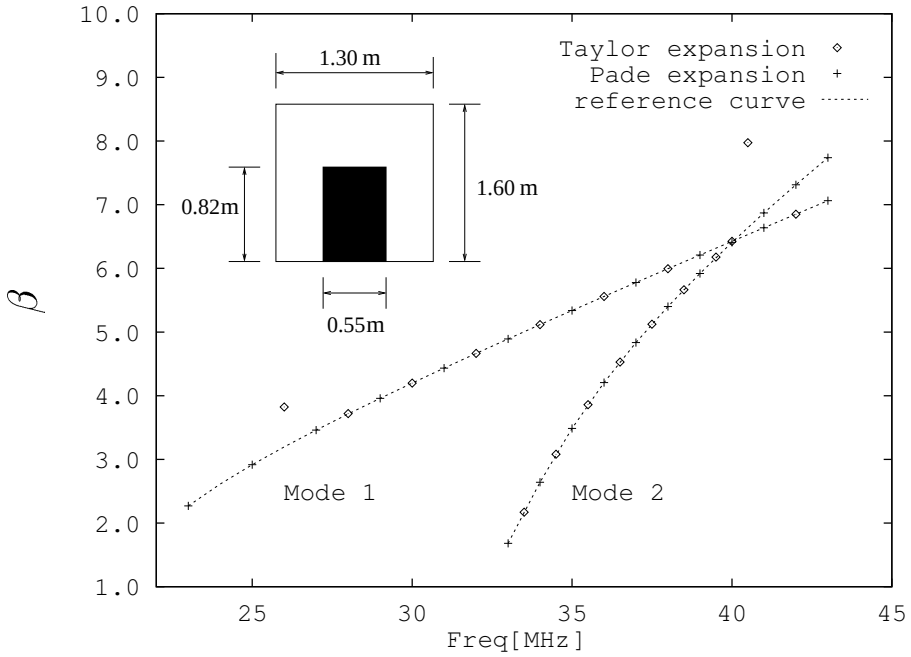

Figure 5: Dispersion curves for the first two modes of the anisotropic waveguide. Shown in inset is the geometry of the anisotropic dielectric waveguide, $\epsilon_{rx} = 170$, $\epsilon_{ry} = \epsilon_{rz} = 85$.

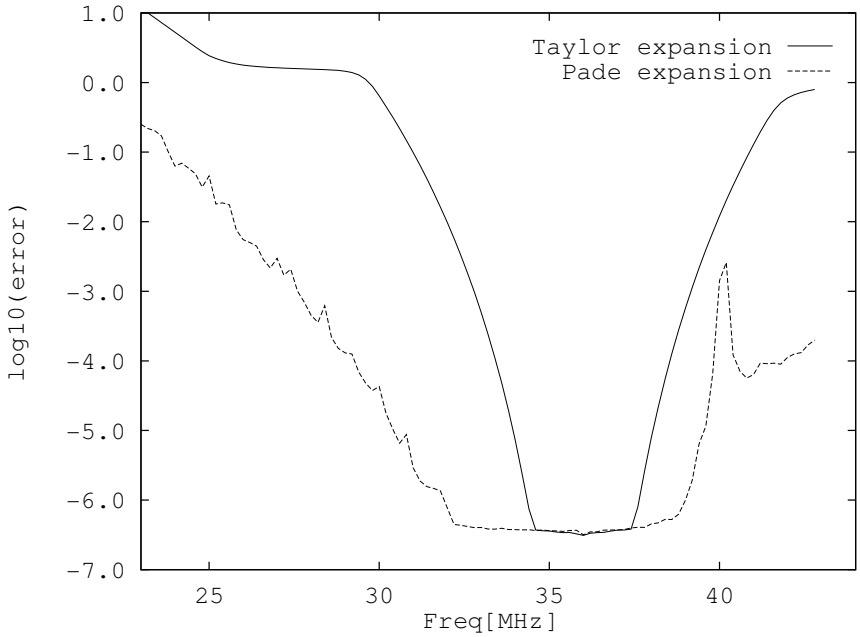

Figure 6: Error versus frequency for the dominant mode of the anisotropic waveguide for the central frequency $f_0 = 36$[MHz].

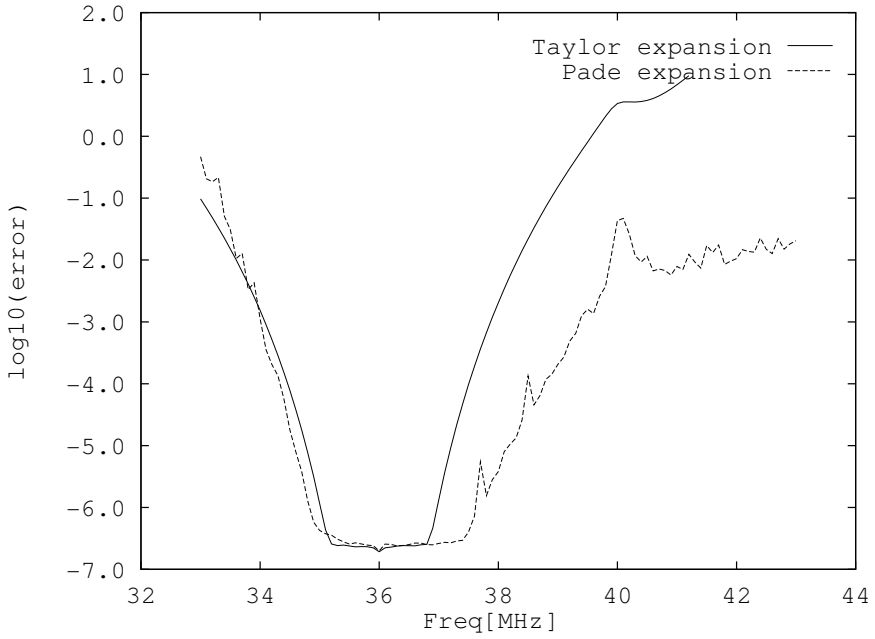

Figure 7: Error versus frequency for the second mode of the anisotropic waveguide for the central frequency $f_0 = 36$[MHz].

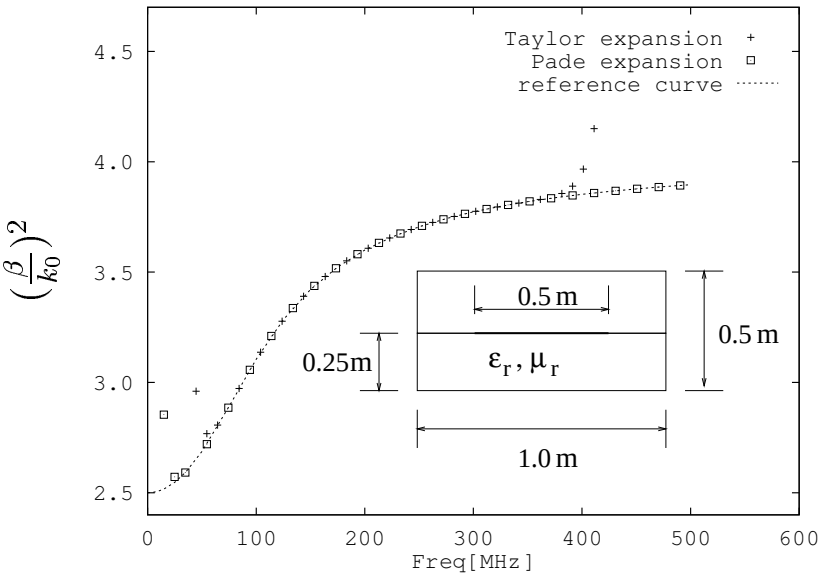

Figure 8: Dispersion curves for the shielded microstrip line corresponding to the central frequency $f_0 = 200$MHz. Shown in inset is the geometry of the microstrip line.

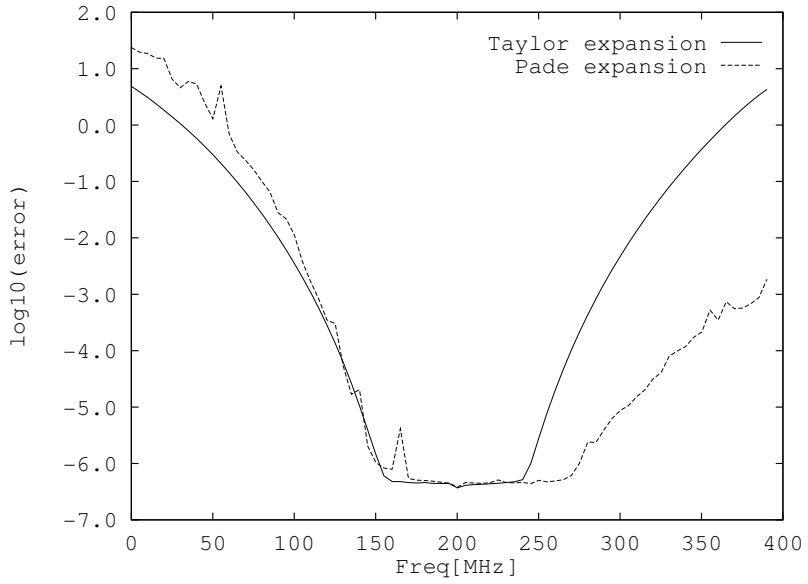

Figure 9: Error versus frequency for the microstrip line for $f_0 = 200$MHz.

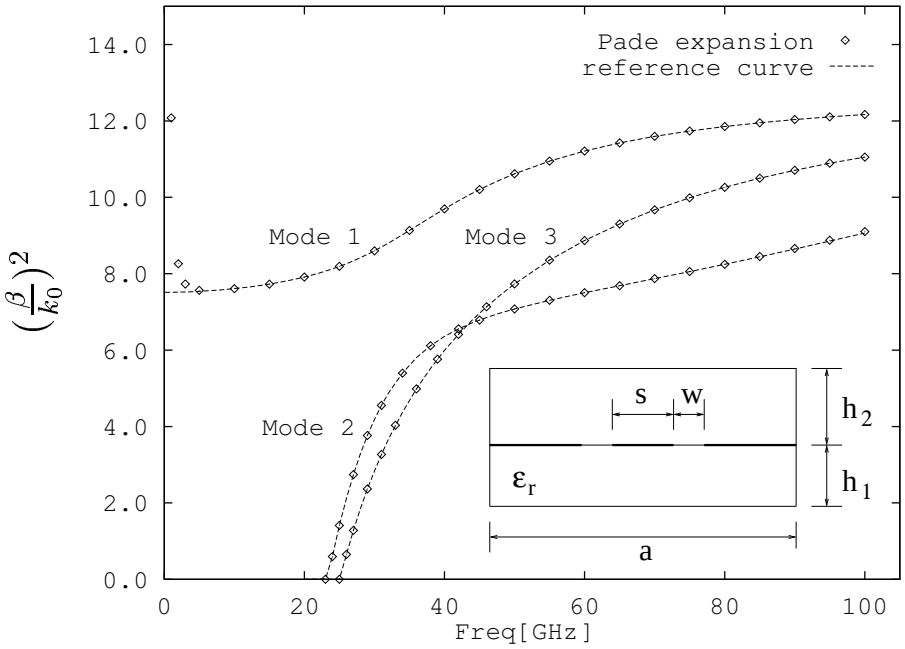

Figure 10: The dispersion curves for the first three modes for the structure shown in inset with dimensions $w = 0.2mm$, $a = 2mm$, $h_1 = 0.2mm$, $h2 = 0.6mm$, $s = 0.1mm$, and $\epsilon_r = 12.9$. Padé expansion has been obtained based on the known modes characteristics for the central frequency $f_0 = 35GHz$.